ELSEVIER

Journal of Wind Engineering
and Industrial Aerodynamics 93 (2005) 155–169

JOURNAL OF wind engineering AND industrial aerodynamics

www.elsevier.com/locate/jweia

Wind tunnel tests of effects of atmospheric stability on turbulent flow over a three-dimensional hill

Takeo Takahashi[a,*], Shinsuke Kato[a], Shuzo Murakami[b], Ryozo Ooka[a], Mohamed Fassy Yassin[c], Ryohei Kono[a]

[a]*Institute of Industrial Science, The University of Tokyo, 4-6-1, Komaba, Meguro-ku, Tokyo 153-8505, Japan*
[b]*Faculty of Science and Technology, Keio University, 3-14-1, Hiyoshi, Kohokiu-ku, Yokohama 223-8522, Japan*
[c]*Faculty of Engineering, Assiut University, Assiut-71516, Egypt*

Received 29 July 2003; received in revised form 27 September 2004; accepted 18 November 2004
Available online 29 December 2004

Abstract

This paper presents a wind tunnel study on the turbulent structure of the airflow around a three-dimensional hill model placed in a boundary-layer flow. The effect of atmospheric stability: stable, neutral and unstable on the flow field of the boundary layer is examined. The wind velocity is measured with a three-dimensional laser doppler anemometer (LDA). Measurements analysis includes mean velocity, turbulent velocity, Reynolds stress and turbulence energy profiles around the hill. The main results are as follows: (1) The mean wind velocity does not vary with the stability at the hilltop; it reaches a maximum at the back of the hill, for the unstable case. (2) The turbulent velocity at the back of the hill reaches its peak value at the height of the hilltop. It takes maximum value for the stable boundary layer flow, and become smaller for the neutral flow and the unstable flow. Buoyancy production has little effect on the turbulence energy. (3) A clear peak of $-\overline{u'w'}/U_H^2$ is observed at a height near $Z/H = 1$. The peak value becomes the largest for the stable case and the smallest for the unstable case.

Keywords: Wind tunnel tests; Three-dimensional hill; Turbulence flow; LDA; Atmospheric stability

*Corresponding author. Tel.: +81 3 5452 6431; fax: +81 3 5452 6432.
E-mail address: aa51702@iis.u-tokyo.ac.jp (T. Takahashi).

0167-6105/$ - see front matter © 2004 Elsevier Ltd. All rights reserved.
doi:10.1016/j.jweia.2004.11.003

Nomenclature

H	height of the hill model (= 200 mm)
L	diameter of the hill model at the base (= 840 mm)
L_o	height of hill model from the floor surface (mm)
Z	height from the model surface (mm)
X	distance in the longitudinal direction ($X = 0$ means the center of the model)
U	mean velocity in the longitudinal direction
U_H	mean velocity at the height of the model
$\sqrt{\overline{u'^2}}$, $\sqrt{\overline{v'^2}}$, $\sqrt{\overline{w'^2}}$	turbulent velocity
k	turbulent energy ($= 1/2(\overline{u'^2} + \overline{v'^2} + \overline{w'^2})$)
R_i	bulk Richardson number $= (1/F_r)$ ($= gH(T_H - T_S)/\theta_H U_H^2$)
θ_H	absolute temperature of T_H
T_H	temperature at a height H
T_S	temperature at the floor surface
g	gravitational acceleration

1. Introduction

There is a need to develop a local wind prediction model in order to make use of wind energy. The prediction model should be usable for mountainous and steep terrains in Japan, and data are needed to validate the prediction model. The characteristics of turbulence flow over complex terrains have been well investigated [1–9], but there have been few studies in stable and unstable conditions. In this study, turbulent flow characteristics around a three-dimensional hill are investigated with a thermally stratified wind tunnel. The result of these wind tunnel tests provide not only the mean velocity and temperature distributions, but also the turbulence characteristics of the three-dimensional velocity fields for flows over a three-dimensional hill with an isolation peak in stable, neutral and unstable atmospheric boundary layers.

2. Overview of the experiment

2.1. Wind tunnel

A thermally stratified wind tunnel with a closed circuit was used. The working section is 2.2 m wide, 1.8 m high, and 16.5 m long (Fig. 1). An air cooling device is installed upwind of the contract section. The air temperature is controllable in the range 12–35 °C. The entrance to the working section (just behind the contract

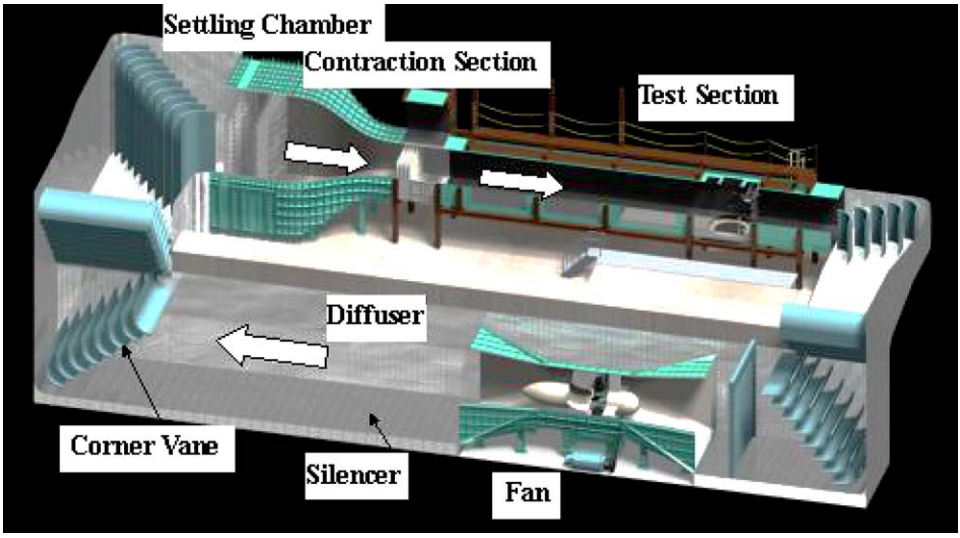

Fig. 1. Wind tunnel.

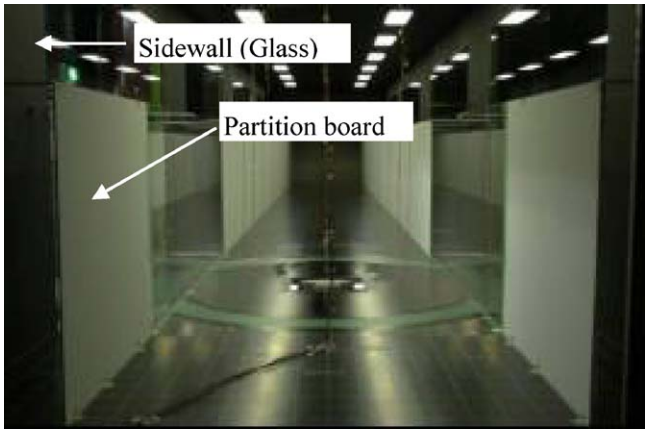

Fig. 2. Inside view of working section.

section) is partitioned into 40 layers in the perpendicular direction. Each layer is 45 mm thick, and has a heater. The temperature is controlled in the range of 12–50 °C. The floor of the working section is partitioned into six parts. Each part can be heated or cooled individually. To protect against the cold draft from the sidewall, which is made of glass, and to ensure a two-dimensional flow, we place partition boards about 900 mm high along the tunnel sidewall. They are separated from the sidewall by 200 mm (Fig. 2).

2.2. Terrain model

An axial symmetric hill model is used (Figs. 3 and 4). The scale of the model is 1/1000. The shape of the cross section is defined by $L_o = 0.5H^*(1 + \cos(2\pi X/L))$. It is 200 mm high, with 840 mm base. Tripping wires to make the model surface rough, we attach 1 mm-square pipes to the surface of the model in concentric circles, with the pitch maintained at 50 mm.

2.3. Velocity measurements

The components of the wind velocity in the wind tunnel are measured with a three-dimensional Laser Doppler Anemometer (LDA). To make measurements with this

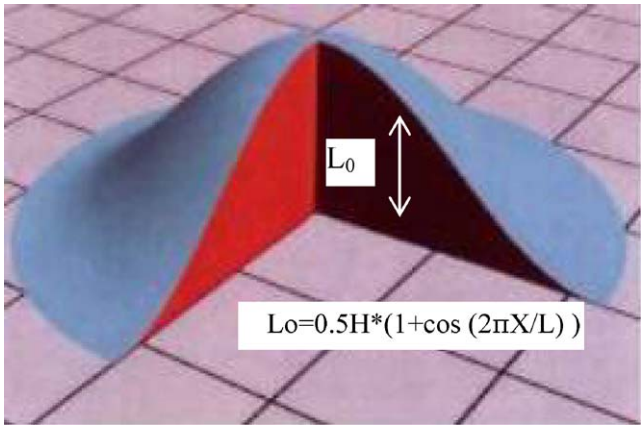

Fig. 3. Terrain model: three-dimensional hill.

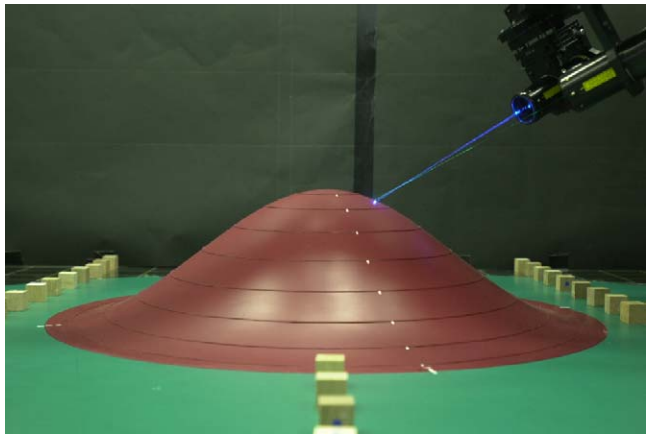

Fig. 4. Installed model in wind tunnel.

instrument, oil mist particles are seeded into the flow. Two lenses are mounted on a sensor traverse unit in the direction looking upwind from the downwind side; one for measuring the wind velocity's U and W components, and one for measuring the V component. Each lens has a focal length of 400 mm, a probe diameter of 60 mm, and a probe length of 250 mm. The laser beams from the two lenses cross at an included angle of 60° in the horizontal plane, and the dip angle is 30° in the vertical plane (Figs. 5 and 6). The separate wind velocity components are calculated by coordinate transformation. Because the LDA probe sensors are mounted on the Z-axis of the traverse (moving up and down) in the wind tunnel and have a fixed dip angle, the wind tunnel flow passing through the LDA sensor has a tendency to flow down under the LDA sensor. The measured wind velocity of the W component is thereby a bit lower (negative) compared with the real value without the LDA sensor.

The sampling time for one measurement was about 45 s. It corresponded to the 2000 samples for one measurement. The measured mean velocity scatters within 5% for very low wind velocity and the Reynolds stress scatters within 10%. If the point where the mean wind velocity was extremely small was excluded, it was judged to have enough measurement accuracy.

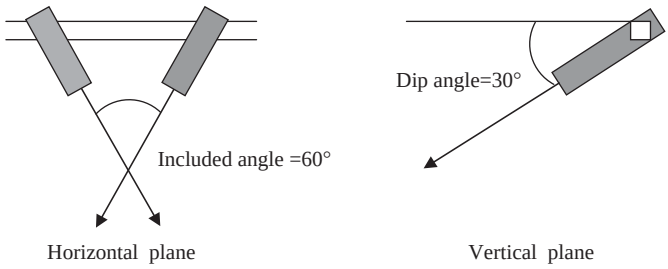

Fig. 5. Arrangement of LDA probe.

Fig. 6. LDA probe.

2.4. Temperature profile

The vertical temperature profiles in the stable case and the unstable case are shown in Fig. 7. During this study, the temperature is automatically controlled to give a maximum error of $\pm 0.5\,^{\circ}\mathrm{C}$.

2.5. Velocity profile

The boundary layer flow is simulated using three spires 1600 mm high and three roughness elements ($90 * 90 * 90$, $60 * 60 * 60$, $30 * 30 * 30$, Fig. 8). The mean wind velocity profile is expressed by $U \propto Z^{1/7}$ at $X = 0$ (the center of the model installation point) in neutral conditions. In stable and unstable conditions, the profiles are simulated with the same arrangement of spires and roughness blocks, and become slightly changed from the neutral case (Fig. 9). The height of the boundary layer is about 600 mm, which is about three times as high as the model. At the point on the model, ($X = 0$), the boundary layer is in the course of development; in neutral conditions without the model, the non-dimensional rate of change of the average wind velocity along the flow direction, $\partial U/U_{\mathrm{H}}/\partial X/H$, is 0.008 at the height of the model, indicating attenuation. The experiment wind velocity ranges from 1.2 to 1.4 m/s.

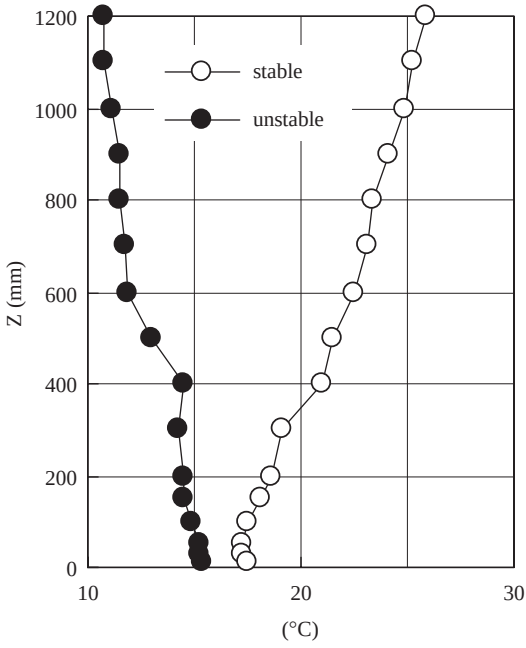

Fig. 7. Vertical distribution of temperature of incident flow at center of turn-table without model ($X = 0.0$ m)

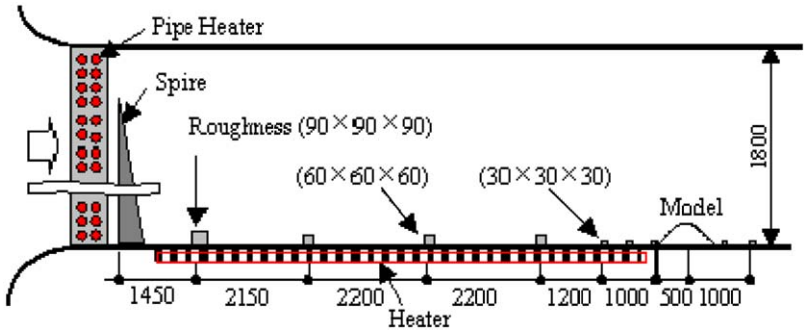

Fig. 8. Arrangement plan of spire, roughness, and heater to simulate a boundary layer.

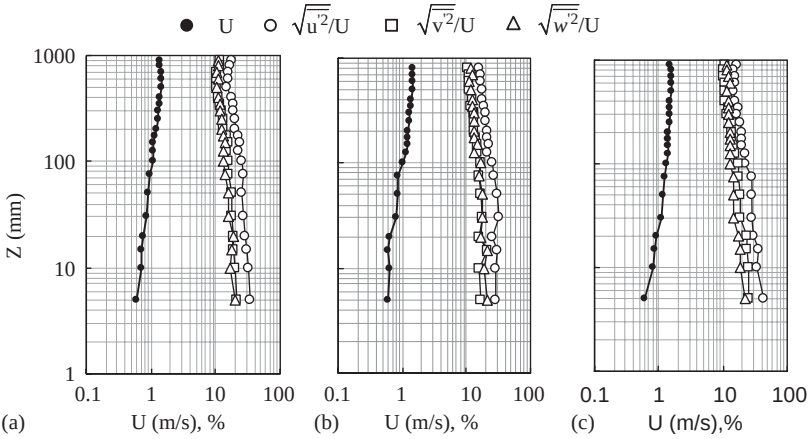

Fig. 9. Vertical distribution of mean velocity and turbulent intensity of incident flow: (a) Stable case, (b) Neutral case, (c) Unstable case.

2.6. Atmospheric stability

The atmospheric stability is evaluated with the Bulk Richardson number $Ri(= gH(T_H - T_S)/\theta_H U_H^2)$. For the present experiments, the number is about 0.008 for stable conditions and about -0.002 for unstable conditions, meaning weakly stable and weakly unstable, respectively.

2.7. Remarks

Without the hill model, the gradient of the temperature boundary layer between the wind tunnel floor and the hilltop ($Z = 200$ mm) at the model placement point was about 0.7 °C/m for stable atmospheric conditions and about -1.4 °C/m for unstable atmospheric conditions. The former is considered to be small; the latter is bit large

and shows a tendency towards boundary layer recovery. The W component is usually suppressed for stable atmospheric conditions and this is true for this experiment. However, in this study for unstable atmospheric conditions, the downward component in the Z-axis at the mean flow became large. This was caused by cool air coming from the upper layer to just over the floor at the point of the model due to the wind tunnel floor heating configuration; a floor heater was placed exactly at the upwind part of the tunnel to the model to create an unstable layer, and the downward part of the tunnel of the model was kept thermally insulated and was not heated.

3. Results

The results are shown using non-dimensional parameters derived by H, the height of the model and U_H, the wind velocity at the height of the model at the point $X/H = 0$ without the model. U_H is different for stable, neutral, and unstable conditions. The height of the lowest measuring point is $Z/H = 0.025$ (5 mm from surface).

3.1. Mean wind velocity distribution, U/U_H

The distributions of U/U_H are shown in Fig. 10. At the point of the hilltop ($X/H = 0$), $U/U_H = 1.31$ in the stable case, $U/U_H = 1.26$ in the neutral case, and $U/U_H = 1.31$ in the unstable case at the lowest measuring point. No large differences are observed between them. At the back of the hill, U/U_H becomes larger for the unstable case, followed by the neutral case; U/U_H becomes smaller for the stable case at the measuring height equal to or less than H. For example, at the point $X/H = 1.125$, $U/U_H = 0.37$ for the stable case, $U/U_H = 0.59$ for the neutral case, and

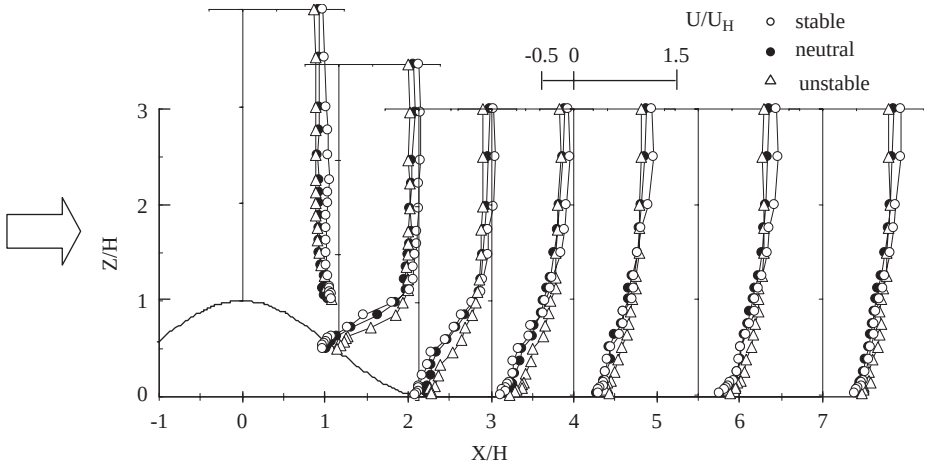

Fig. 10. Vertical profile of mean velocity U/U_H in the central plane of the hill.

$U/U_H = 0.83$ for the unstable case at the height of the model. This feature is explained well by the mixing characteristics of the stability of the boundary layer. Inverse flows are observed in the wake region in all cases. In both the stable and neutral cases, an inverse flow is observed up to a height of $Z/H = 0.15$. In the unstable case, an inverse flow is barely observable at a height of $Z/H = 0.025$. Downstream of the point $X/H = 2.25$, an inverse flow is observed only in the stable case.

3.2. Mean wind velocity distribution, W/U_H

The distributions of W/U_H are shown in Fig. 11. Although the absolute value is small, a downward wind is observed over the hilltop in all cases. It is difficult to physically explain this downward stream, and the method adopted to mount the LDA probe (coordination with the wind tunnel coordinate system) introduces a systematic inaccuracy as previously stated (2.3). For this reason, the following discussion will be limited to a comparison of the atmospheric stability. W/U_H gives large negative values in wide areas at the back of the hilltop; this means a stronger downward flow. Near the floor, however, the downward flow becomes small. At the region of under $Z/H = 1$ and $X/H = 0$ ranges from 0 to 2.25, the absolute value of W/U_H in the case of unstable is larger than the case of neutral, that in the case of stable is smaller than the case of neutral. For a range of $X/H > 4$, W/U_H is not affected by changes in the atmospheric stability.

3.3. Turbulent intensity distribution, $\sqrt{\overline{u'^2}}/U_{H\square}\sqrt{\overline{v'^2}}/U_{H\square}\sqrt{\overline{w'^2}}/U_H$

The distributions of turbulent velocity are shown in Figs. 12–14. At the back of the hill ($X/H = 1.125, 2.25$), $\sqrt{\overline{u'^2}}/U_H$, $\sqrt{\overline{w'^2}}/U_H$ have their peak values at the height of

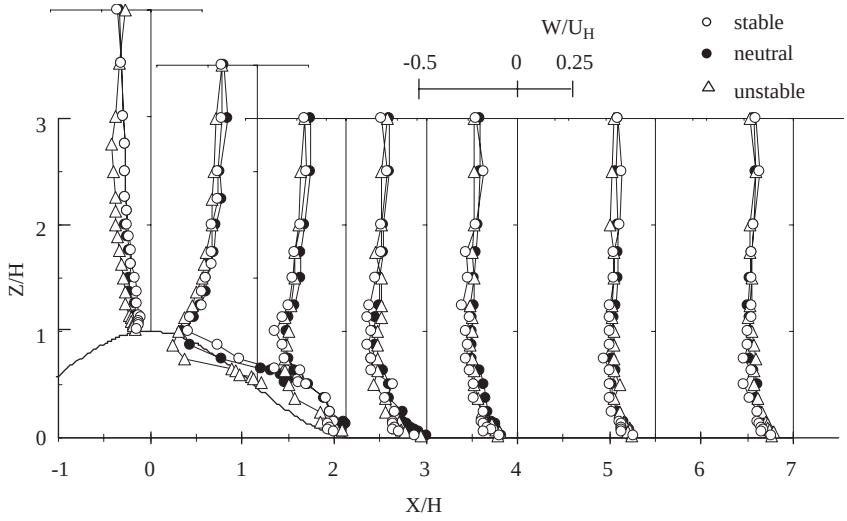

Fig. 11. Vertical profile of mean velocity W/U_H in the central plane of the hill.

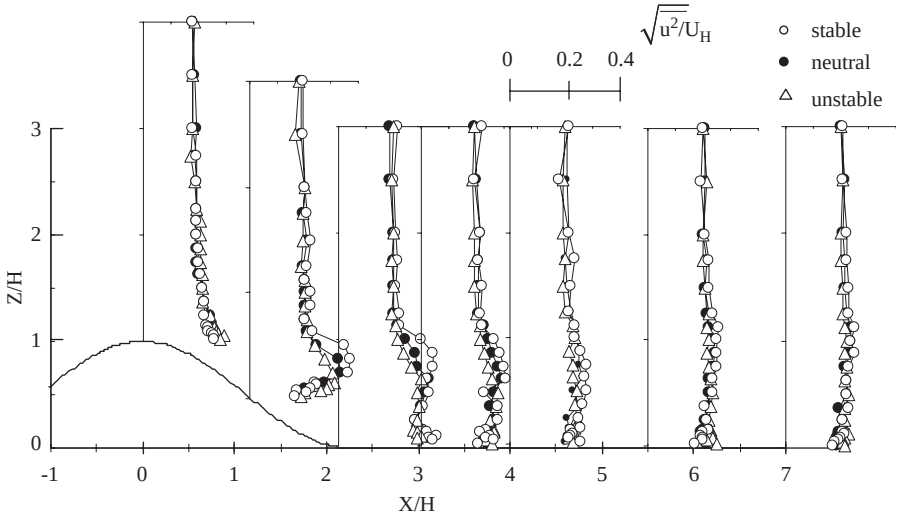

Fig. 12. Vertical profile of turbulent velocity $\sqrt{\overline{u'^2}}/U_{\mathrm{H}}$ in the central plane of the hill.

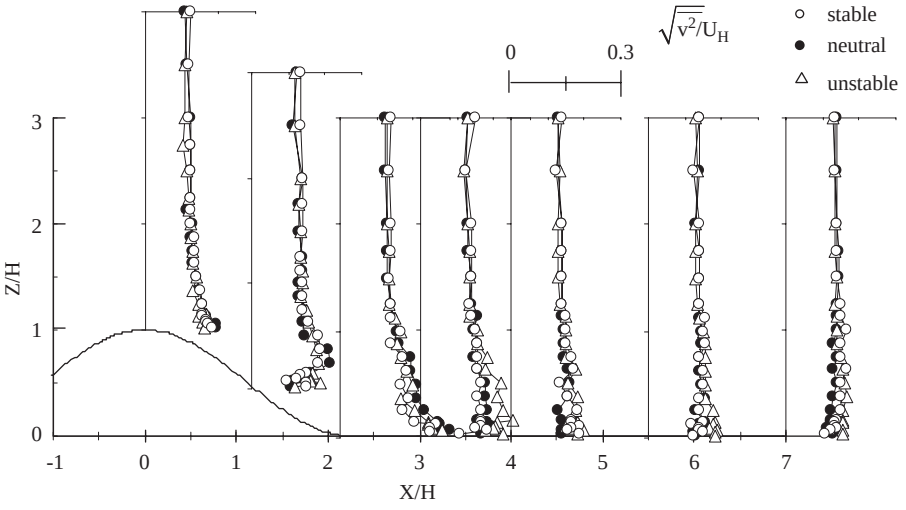

Fig. 13. Vertical profile of turbulent velocity $\sqrt{\overline{v'^2}}/U_{\mathrm{H}}$ in the central plane of the hill.

the hill. The point of the peak corresponds to the point where the velocity gradient becomes the largest. These results are consistent with the previous results [8]. The peak of $\sqrt{\overline{u'^2}}/U_{\mathrm{H}}$ has its largest value for the stable case, with the neutral case coming next. It becomes smaller for the unstable case. The position of the peak is highest for the stable case and the lowest for the unstable case. This corresponds to the vertical gradient of the mean flow. At the point $X/H = 1.125$, the position of the

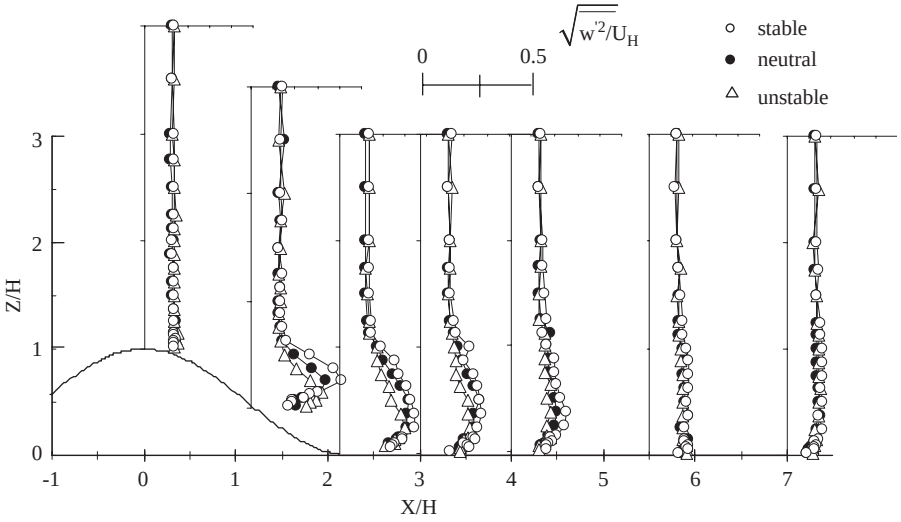

Fig. 14. Vertical profile of turbulent velocity $\sqrt{\overline{w'^2}}/U_H$ in the central plane of the hill.

peak and its value are as follows: $Z/H = 0.375$ and 0.37 for the stable case, $Z/H = 0.25$ and 0.34 for the neutral case, and $Z/H = 0.15$ and 0.32 for the unstable case.

The results of the distribution of $\sqrt{\overline{v'^2}}/U_H$, do not show a clear distinction despite the variations in atmospheric stability. This is not the case for $\sqrt{\overline{u'^2}}/U_H$. At the back of the model (near $X/H = 2.25$ and 3.0), $\sqrt{\overline{v'^2}}/U_H$ had its large values near the floor. This phenomenon, showing the strong effect of currents flowing along the model, was not observed for $\sqrt{\overline{u'^2}}/U_H$ and $\sqrt{\overline{w'^2}}/U_H$.

The distribution of $\sqrt{\overline{w'^2}}/U_H$ is similar to that of $\sqrt{\overline{u'^2}}/U_H$, having the largest peak for the stable case. This result shows that the gradient of the mean flow contributes more than the buoyancy to the production of turbulence. The position of the peak is the highest for the stable case and lowest for the unstable case. At the points $X/H = 5.5$ and 7.0, however, there is no effect from the atmospheric stability.

3.4. Turbulence energy distribution, k/U_H^2

The distributions of turbulent energy are shown in Fig. 15. The peak is obviously seen near the hillside ($X/H = 1.125$). At the back of the hill ($X/H = 2.25$), the peak is close to the floor surface in the wake region.

3.5. Reynolds stress distribution, $-\overline{u'w'}/U_H^2$, $-\overline{u'v'}/U_H^2$, $-\overline{v'w'}/U_H^2$

The distributions of Reynolds stress are shown in Figs. 16–18 corresponding to that was measured because the W component is negative in the upper regions of the

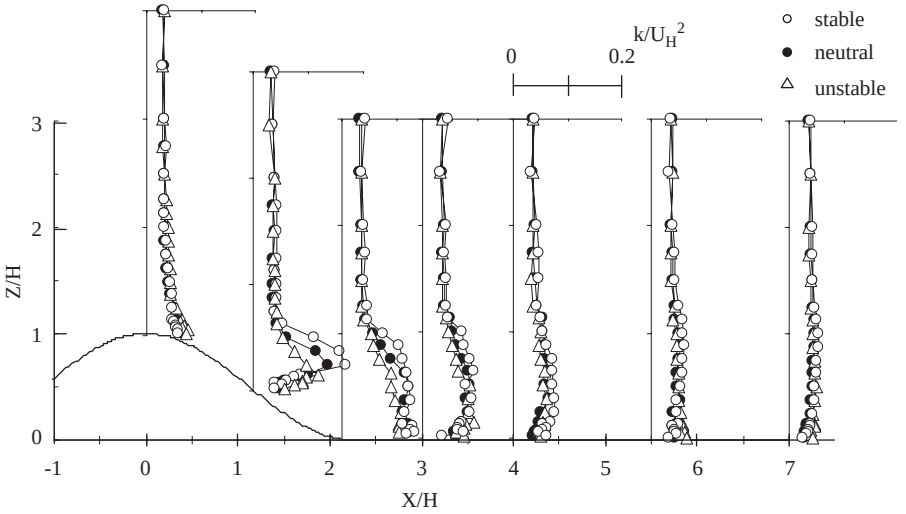

Fig. 15. Vertical profile of turbulence energy k/U_H^2 in the central plane of the hill.

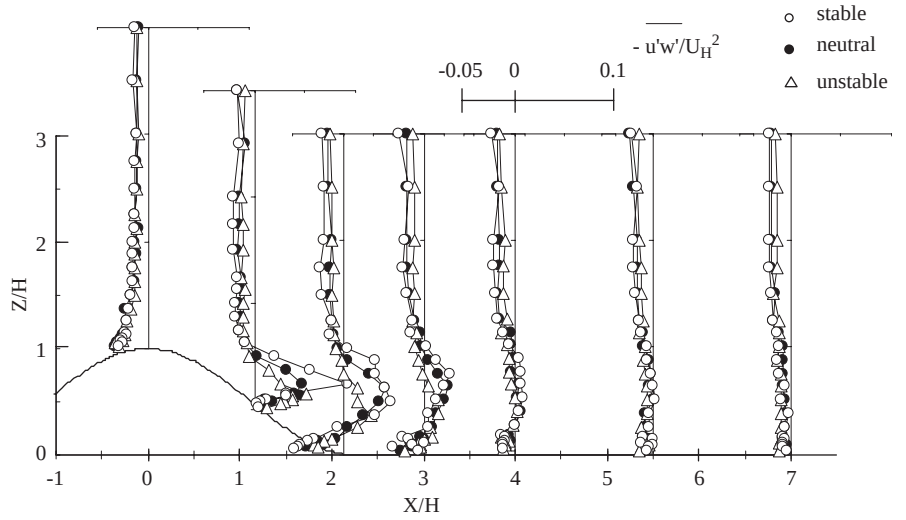

Fig. 16. Vertical profile of Reynolds stress $-\overline{u'w'}/U_H^2$ in the central plane of the hill.

model, $-\overline{u'w'}/U_H^2$ shows the value of negative even. $-\overline{u'w'}/U_H^2$ has a clear peak near $Z/H = 1$, like in the case of the distribution of energy k. It has the largest value for the stable case and the smallest value for the unstable case. The point where the peak appears is the highest for the stable case and the lowest for the unstable case. At the back of the hill of $X/H = 3$, $-\overline{u'w'}/U_H^2$ shows little differences despite variations in the atmospheric stability.

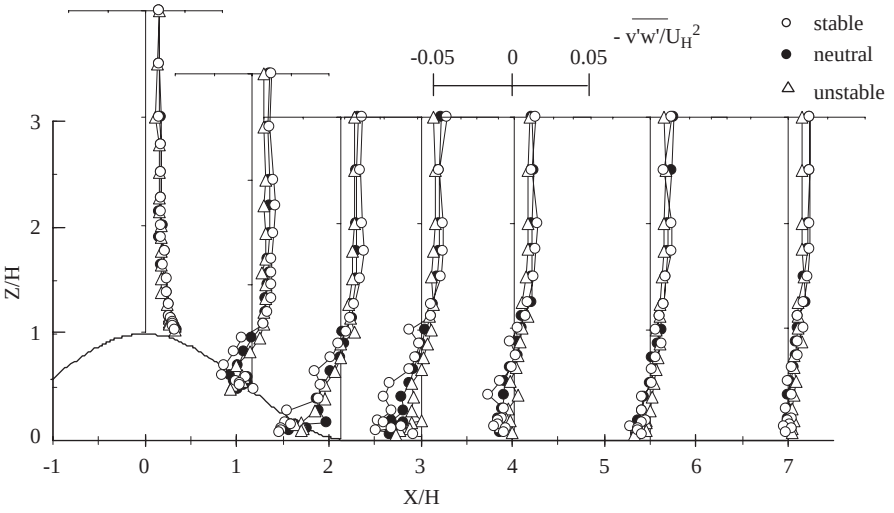

Fig. 17. Vertical profile of Reynolds stress $-\overline{v'w'}/U_H^2$ in the central plane of the hill.

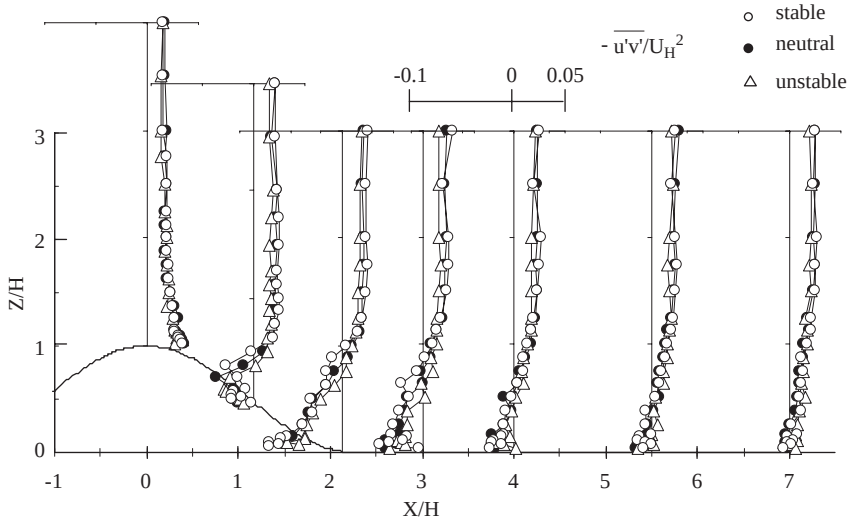

Fig. 18. Vertical profile of Reynolds stress $-\overline{u'v'}/U_H^2$ in the central plane of the hill.

$-\overline{u'v'}/U_H^2$ shows the peak value near the floor surface at $X/H = 2.25$, 3 in the model backward. There is not almost the difference by the change of atmosphere stability in after $X/H = 4$.

$-\overline{u'v'}/U_H^2$ and $-\overline{u'w'}/U_H^2$ shows almost the similar trend.

4. Summary

The turbulence statistical parameters of the airflow over a three-dimensional hill were studied in different atmospheric conditions. The following results are obtained:

(1) Mean wind velocity, U/U_H does not vary at the top of the hill for different atmospheric conditions. At the back of the hill, it has the largest value for the unstable case and the smallest for the stable case at the height below $Z/H = 1$.
(2) At the back of the hill, $\sqrt{\overline{u'^2}}/U_H$ and $\sqrt{\overline{w'^2}}/U_H$ have a peak around the height of the hill. The peak position corresponds to the point where the vertical gradient of U/U_H becomes large.
(3) The peak values for $\sqrt{\overline{u'^2}}/U_H$ and $\sqrt{\overline{w'^2}}/U_H$ become larger for the stable case and smaller for the unstable case. Little effect is observed with the buoyancy production. The position of the peak is higher for the stable case and lower for the unstable case.
(4) $\sqrt{\overline{v'^2}}/U_H$ and k/U_H^2 becomes largest near the floor at the back of the hill.
(5) A clear peak of $-\overline{u'w'}/U_H^2$ is observed at a height near $Z/H = 1$. The peak value becomes the largest for the stable case and the smallest for the unstable case.
(6) The distributions of $-\overline{u'v'}/U_H^2$ and $-\overline{v'w'}/U_H^2$ do not vary greatly with atmospheric stability.
(7) Problems with measuring methods remain unsolved.

Acknowledgement

This research was carried out as part of the research project "Development of a Local Wind Energy Prediction Model" supported by NEDO (New Energy and Industrial Technology Development Organization).

References

[1] E.J. Plate, C.W. Lin, The velocity field downstream from a two-dimensional model hill, Part I, Colorado State University, Fluid Dynamics and Diffusion, Laboratory Report No. CER65EJP14, 1965.
[2] T. Ishihara, K. Hibi, An experimental study of turbulent boundary layers over steep hills, Proceedings of the 15th National Symposium on Wind Engineering, 1988.
[3] G.P. Almeida, D.F.G. Durao, M.V. Heitor, Wake flows behind two-dimensional model hills, Exp. Therm. Fluid Sci. (1993).
[4] P. Scirputowski, J. Ostrowski, A. Cenedese, Experimental study of wind flow over the model of a valley, J. Wind Eng. Ind. Aerodyn. (1995).
[5] Y. Meng, K. Hibi, Turbulent characteristics of flow field over a three-dimensional steep hill, J. Wind Eng. Ind. Aerodyn. (1997).
[6] T. Ishihara, K. Hibi, S. Oikawa, A wind tunnel study of turbulent flow over a three-dimensional steep hill, J. Wind Eng. Ind. Aerodyn. (1999).
[7] Takeshi Ishihara, Measurements and predictions of local wind field in complex terrain, The Fifth Asia-Pacific Conference on Wind Engineering, Kyoto, 2001, p. 9.

[8] Takeshi Ishihara, Yozo Fujino, Kazuki Hibi, A wind tunnel study of separated flow over a two-dimensional ridge and a circular hill, The Fifth Asia-Pacific Conference on Wind Engineering, Kyoto, 2001, p. 9.
[9] T. Takahashi, T. Ohtsu, M. F. Yassin, S. Kato, S. Murakami, Turbulence characteristics of wind over a hill with a rough surface, J. Wind Eng. Ind. Aerodyn. (2002).